Superexchange Charge Transport in Loaded Metal Organic Frameworks

Tobias Neumann,[†,⊥] Jianxi Liu,[‡,⊥,∥] Tobias Wächter,[§,⊥] Pascal Friederich,[†] Franz Symalla,[†] Alexander Welle,[‡] Veronica Mugnaini,[‡,¶] Velimir Meded,[†] Michael Zharnikov,[§] Christof Wöll,[‡] and Wolfgang Wenzel*[,†]

[†]Institute of Nanotechnology (INT) and [‡]Institute of Functional Interfaces (IFG), Karlsruhe Institute of Technology (KIT), 76344 Eggenstein Leopoldshafen, Germany

[§]Applied Physical Chemistry, Heidelberg University, 69120 Heidelberg, Germany

ABSTRACT: **In the past, nanoporous metal−organic frame works (MOFs) have been mostly studied for their huge potential with regard to gas storage and separation. More recently, the discovery that the electrical conductivity of a widely studied, highly insulating MOF, HKUST 1, improves dramatically when loaded with guest molecules has triggered a huge interest in the charge carrier transport properties of MOFs. The observed high conductivity, however, is difficult to reconcile with conventional transport mechanisms: neither simple hopping nor band transport models are consistent with the available experimental data. Here, we combine theoretical results and new experimental data to demonstrate that the observed conductivity can be explained by an extended hopping transport model including virtual hops through localized MOF states or molecular superexchange. Predictions of this model agree well with precise conductivity measurements, where experimental artifacts and the influence of defects are largely avoided by using well defined samples and the Hg drop junction approach.**

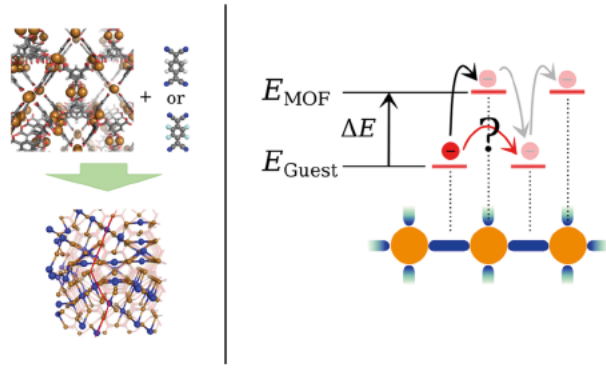

KEYWORDS: *metal−organic frameworks, thin films, guest loading, TCNQ, electric transport properties, mercury based tunneling junctions*

During the past decade,[1−3] nanoporous materials consisting of metal centers linked by organic ligands, so called metal−organic frameworks (MOFs), have attracted enormous attention regarding technological applica tions such as hydrogen storage,[4,5] CO_2 capture,[6,7] catalysis,[8,9] sensing,[10] and photovoltaics.[11] A major advantage of these nanoporous, crystalline solids is that they can be synthesized in a straightforward fashion.[12,13] Today, the number of known MOF structures exceeds 20 000.[2] One key challenge with respect to applications involving charge transport has been the poor electrical conductivity of MOFs, which results from the sizable electronic band gap present in most MOF com pounds.[14] In addition, the mobility of (photo)excited charge carriers is low, a consequence of the flat electronic bands present in many systems.[15] Recently, an increase in electrical conductivity of up to 6 orders of magnitude has been reported when HKUST 1, a widely studied porous, crystalline, and wide band gap semiconductor, is loaded with 7,7,8,8 tetracyanoqui nodimethane (TCNQ).[16] Interestingly, for the analogous fluorinated compound, F4 TCNQ, the increase in conductivity was observed to be much smaller.[16] Closer inspection of this breakthrough toward applications requiring conductive MOFs raises several questions. In particular, the nature of the transport mechanism has remained unclear. Obviously, with regard to future integration of MOF based components in electronic devices, the basic principles governing charge transport in these novel and exciting materials need to be understood in more detail.

For metals and inorganic semiconductors, the accepted model for electrical conductivity is band transport of delocalized charge carriers. Electronic transport in strongly disordered amorphous semiconductors, on the other hand, is described in terms of hopping models assuming localized charge carriers.[17,18] The temperature dependence predicted by these two mechanisms is fundamentally different: in band transport, increasing temperature reduces the conductivity due

to increased electron (or hole)−phonon scattering, while activation barriers govern hopping transport, thus increasing the conductivity with temperature. In previous work, activated transport has been reported in HKUST 1 loaded with TCNQ (activation energy 41 meV). Both electron and hole transport models[19] have been proposed to account for the experimentally observed, fairly large conductivities.[16] With respect to the nature of the carriers, Seebeck measurements[19] indicate hole transport in the context of a band model. We note, however, that loading the crystalline MOF with guest molecules induces disorder in the system. The sign of the Seebeck coefficient is determined by the difference between Fermi level and the level of a localized density of states. In the presence of orientation disorder, which in loaded HKUST 1 arises from the different possible orientations of TCNQ in the pore, the transport energy may be shifted above or below the Fermi level. As a result, the sign of the Seebeck coefficient[19] may not uniquely determine the nature of the carrier,[20] complicating the interpretation of this experiment.

In the following, we will therefore discuss models considering both hole and electron hopping transport in TCNQ loaded HKUST I in the context of previous and new experimental data. We first note that it is difficult to understand the electronic transport through the loaded MOF in terms of classical hopping models because the conductivity of the loaded MOF (6 S/m[16]) rivals that of well conducting organic crystals.[21] In the latter class of compounds, the hopping transport of charge carriers depends on the electronic coupling $J_{a,b}$ between adjacent molecules, which drops exponentially with the distance between hopping centers. The distance between such sites (1.3 nm for guest molecules in neighboring MOF pores) is substantially larger than typical distances between molecules in an organic solids (~0.5 nm),[22,23] and as a result, rates for direct hopping between guest molecules in the MOF, as illustrated in Figure 1a (solid blue line), should be very small. Models considering hopping between guest molecules thus predict a conductivity in the loaded MOF much smaller than that in densely packed organic crystals. Direct hopping between the MOF host sites (Figure 1a, solid orange line) can be excluded because of the low conductivity of the unloaded

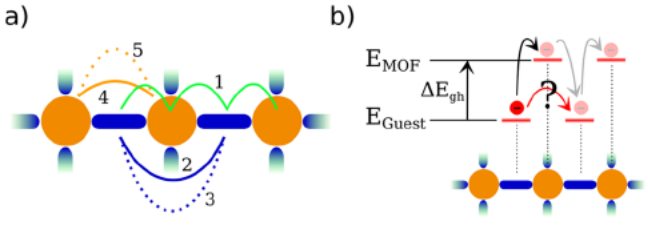

Figure 1. Charge transfer in guest−MOF systems *via* hopping processes. (a) Possible first order transfer processes (solid lines) in a MOF−guest system are the subsequent hopping between guest and MOF sites (1) and the direct transfer between guest−guest or MOF−MOF sites (2,4). Processes (1) and (2) are suppressed by large ΔE and low J, respectively, and the rate of process (4) is limited because MOF states are not occupied. In order to explain high current densities in the MOF−guest system, additional second order processes (superexchange, dashed lines) are consid ered (3,5). (b) Transfer between the LUMO orbitals of the guest molecules can proceed directly or *via* occupancy of a virtual state in the MOF. In the superexchange process, the energy difference, ΔE_{gh}, enters linearly in the rate, while it enters exponentially in guest−host hopping processes.

MOF. We therefore conclude that a simple hopping model cannot explain the TCNQ induced conductivity in a straightforward fashion.

It has been argued[15,16] that the loading of HKUST 1 with organic molecules leads to the formation of additional hopping sites, introduced by the organic molecules bridging the metal centers of the MOF (green lines in Figure 1a). As a result, hopping processes involving subsequent occupation of electronic states localized at MOF sites and states localized at guest sites become possible. As we will show below, the rates describing hopping between sites of different character are extremely low.

The most appropriate theoretical description for the hopping rates between weakly coupled sites (the coupling matrix element is smaller than the activation energy) is Marcus theory[24] (see Methods).

According to this model (eq 1), the hopping rate along a path connecting guest and host sites is vanishingly small because the difference in energy, ΔE_{gh}, between the guest (g) and host (h) sites is about 1 eV for TCNQ loaded HKUST 1. Such a large barrier leads to a pronounced activation energy of E_a ($E_a = \lambda/4(1 + \Delta E_{gh}/\lambda)^2$; *vide infra* for details) and, thus, to a temperature dependence, which is inconsistent with the small temperature induced changes in conductivity observed in the experiment.[16] In fact, an Arrhenius type analysis of the available data[16] results in an apparent activation energy of only 41 meV. We quantitatively show below that neither direct guest−guest nor direct guest−host hopping can explain the large conductivity observed for HKUST 1 loaded with TCNQ.

In view of the failure of simple hopping mechanisms, we next discuss an extension of such first order models that permits charge transfer between next nearest neighbors *via* a second order process referred to as molecular superexchange[25,26] (Figure 1a, dashed orange and blue lines). This mechanism involves a charge transfer between next nearest neighbor guest molecules *via* the virtual occupation of an intermediate state, here, a MOF (or host) state (labeled h).

The derivation of the transfer matrix element between two guest sites including the superexchange mechanism, J_{gg}^{tot}, is given in the Methods section in eq 2. On one hand, as $\Delta E_{gg} \ll \Delta E_{gh}$ and ΔE enters eq 1 as a square exponent, by connecting guest sites, we can avoid the exponential suppression of large site energy differences. On the other hand, the superexchange contribution (J^{sx} in eq 2) contains a product of two hopping rates, which is much smaller than a direct guest−host or host−guest hopping rate. In the following, we perform a quantitative analysis of the material specific parameters for the loaded MOF in order to investigate the relevance of the superexchange process. The calculated rates are used as input for kinetic Monte Carlo (KMC) simulations,[27] which yield quantitative estimates for the charge mobility (see the Supporting Information for details).

RESULTS AND DISCUSSION

In order to investigate the possible scenarios, we have computed the microscopic parameters for both the structure and the electronic properties of HKUST 1 loaded with TCNQ/F4 TCNQ. As a first step, we conducted a systematic search of the possible conformations in which the guest molecule can bind to the metal−organic framework (see the Supporting Information). In addition to the arrangement of the guest molecules in HKUST 1, as proposed by Allendorf *et al.*,[16] two other stable configurations were identified (see Figure S9).

The most stable geometry with binding energies of −1.97 and −1.82 eV for TCNQ and F4 TCNQ, respectively, differs from the previously proposed structure and is displayed in Figure 2. The binding energies of the remaining configurations, as depicted in Figure S9b,c, are −0.99 and −1.25 eV for TCNQ as well as −0.91 and −1.18 eV for F4 TCNQ, respectively.

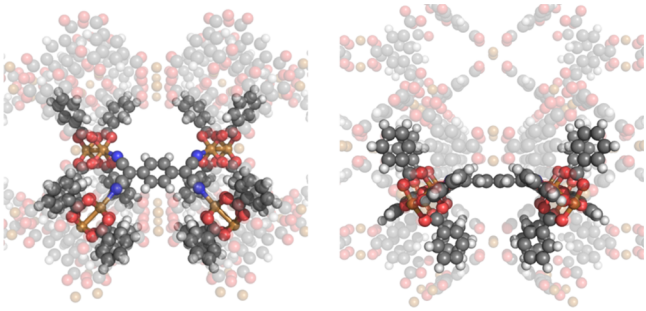

Figure 2. Binding mechanism of F4 TCNQ in HKUST 1: each nitrogen atom of the guest molecules is attached to a copper atom of HKUST 1. The total binding energy is −1.97 eV for TCNQ and −1.82 eV for F4 TCNQ. This configuration is energetically favorable by 0.72 eV for TCNQ and 0.66 eV for F4 TCNQ in comparison to other configurations. In the preferred configuration, each cavity can host up to two guest molecules, resulting in a large number of additional hopping sites in the MOF.

For the lowest energy configuration, we computed the coupling matrix elements of the relevant combinations of LUMO orbitals using the Löwdin orthogonalization method[28] (see the Supporting Information for details). For TCNQ direct guest−guest hopping, we find coupling matrix elements of 1.7 × 10^{-8} and 4.1 × 10^{-9} eV for parallel/orthogonal orientations, respectively, with comparable numbers for F4 TCNQ (all data are given in Table 1). For both configurations, coupling matrix elements are much smaller than the guest−MOF and MOF−MOF couplings, as expected on the basis of the qualitative arguments. The guest−host coupling for F4 TCNQ (2.4 × 10^{-3} eV) is somewhat larger than the coupling for TCNQ (1.4 × 10^{-3} eV) but on the same order of magnitude.

Next, we computed the reorganization energies (λ) using Nelsen's four point method[29] for all relevant hopping sites. We find that reorganization energies for the guest molecules are comparable (∼0.27 eV), whereas reorganization energies of the MOF is considerably larger (∼0.58 eV). If only guest−guest hopping is considered, this results in an activation energy of 67 meV, which is commensurate with the experimentally observed activation energy, while activation energy of hopping processes involving MOF states is much larger. All microscopic data are summarized in Table 1.

The final quantity required to compute the direct and superexchange coupling rates is the site energy differences. It is difficult to quantitatively compute HOMO−LUMO gaps for large systems, such as MOFs, with present state of the art computational methods using (hybrid) (TD)DFT approaches. Computational results on electronic properties of MOFs obtained with DFT methods have been shown to strongly depend on the XC functional used.[30] Hence, calculations of the energy difference, ΔE_{gh}, with any of these methods result in rather large method dependent uncertainties. In agreement with prior work, we estimate ΔE_{gh} > 0.4eV for both guest molecules, but given this uncertainty, we will treat ΔE_{gh} as a parameter in the following discussion and discuss the consequences for the transport in various regimes of ΔE_{gh}. However, we note that for ΔE_{gh} > 0.4 eV the direct process activation energy, E_a, is much larger than 0.42 eV. This cannot be reconciled with the experimental observations[16] and suggests that superexchange may be relevant (for details, see the Supporting Information and Figure S11 therein).

In Figure 3a,b, we show the Marcus transfer rates for all relevant processes calculated with the microscopic parameters as a function of ΔE_{gh}. We find for both guest molecules that the rate for the direct transfer between guest molecules (which is independent of ΔE_{gh}) is orders of magnitude smaller than that for the superexchange processes. This is a direct result of the very small electronic couplings of $J < 10^{-7}$ eV between guest molecules. For ΔE_{gh} < 0.4 eV, the electron transfer is dominated by the direct guest−MOF−guest process, while for ΔE_{gh} < 0.4 eV, the superexchange rate exceeds the rates of the direct processes by several orders of magnitude.

We note that there are 12 different possibilities for a guest molecule to bind in a pore in the configuration shown in Figure 2, with the mobility depending on packing as well as on the microscopic electronic properties. In order to compute the mobility of the materials, we have therefore constructed a model system (for details, see the Supporting Information), where the guest molecules were placed in each cavity according to the optimized geometry with a random orientation within the cavity. We then performed KMC transport calculations using the microscopic hopping rates computed above for all processes and averaged the current over a total of 50 simulations (see the Supporting Information). We find that the charge carrier mobility based on direct hopping is comparable or higher than the superexchange for small guest−host energy mismatch (ΔE_{gh} < 0.4 eV). However, that changes quite dramatically with increasing ΔE_{gh} and beyond the crossing point; superexchange related charge mobility domi nates over the competing processes. Qualitatively similar behavior can be observed for F4 TCNQ. Figure 3c shows the results of KMC simulations: For (ΔE_{gh} > 0.4 eV) super

Table 1. Coupling Matrix Elements between Guest Molecules, Guest Molecule and MOF−Orbital, and MOF−MOF Orbitals and Reorganization Energies (λ) for Guest Molecules and MOF Orbitals[a]

	J (eV)					λ (eV)		
	TCNQ MOF	F4-TCNQ MOF	MOF MOF (first/second nn)	TCNQ TCNQ (o/p)	F4-TCNQ F4-TCNQ (o/p)	TCNQ	F4-TCNQ	MOF
HOMO	1.7 × 10^{-3}	1.4 × 10^{-3}	6.0 × 10^{-4}/7.3 × 10^{-6}	2.0 × 10^{-6}/ 4.3 × 10^{-6}	2.0 × 10^{-8}/4.8 × 10^{-9}	0.129	0.166	0.664
LUMO	1.4 × 10^{-3}	2.4 × 10^{-3}	5.7 × 10^{-2}/3.0 × 10^{-5}	1.7 × 10^{-8}/ 4.1 × 10^{-9}	2.0 × 10^{-8}/5.0 × 10^{-9}	0.266	0.271	0.580

[a]For the coupling between the MOF hopping sites, first and second nearest neighbors are considered. Two different alignments of guest molecules in neighboring cavities (orthogonal, o, and parallel, p) can be observed in the model.

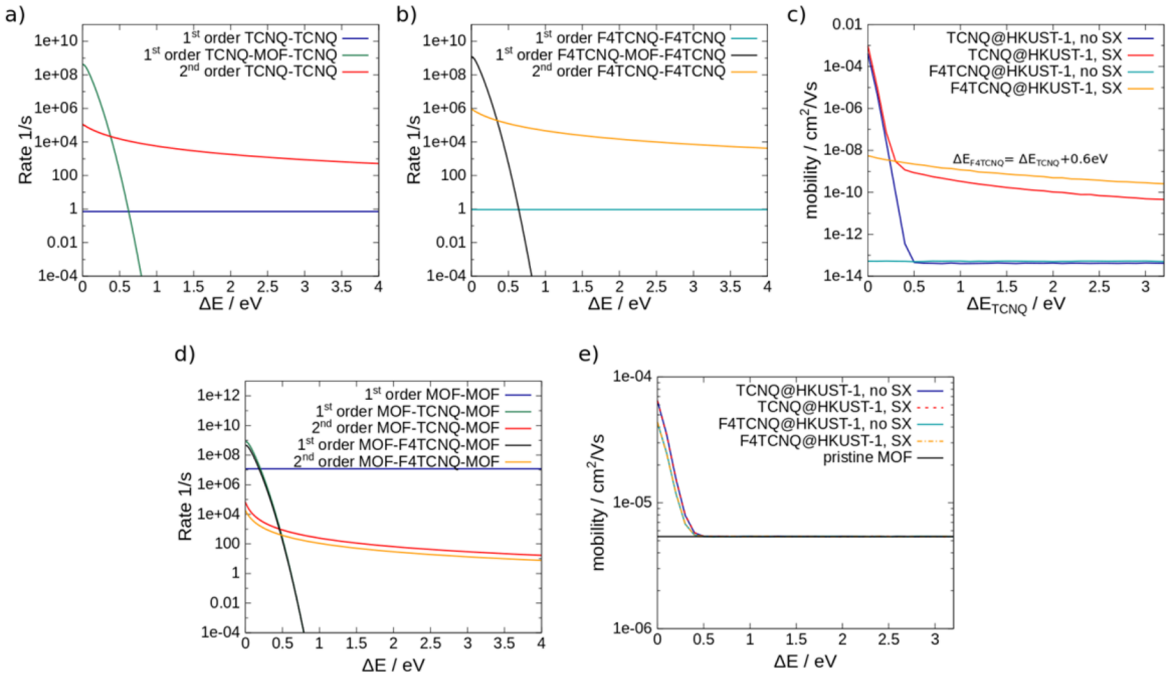

Figure 3. Marcus transfer rates and electron mobility calculated with kinetic Monte Carlo simulations. Marcus transfer rates are calculated for three different transfer processes between guest molecules TCNQ (a) and F4 TCNQ (b) in the MOF: (i) the direct first order charge transfer (blue/cyan); (ii) the first order charge transfer from guest molecule to HKUST 1 and from HKUST 1 onto the subsequent guest molecule (green/black); and (iii) the second order process (superexchange) between guest molecules, where the HKUST 1 intermediate state is only virtually occupied (red/orange). The first order guest−MOF−guest process is predominant for $\Delta E > 0.4$, whereas the superexchange process is orders of magnitude faster for $\Delta E > 0.4$ for both TCNQ and F4 TCNQ. (c) Mobility from KMC simulations with superexchange (sx, red (TCNQ)/orange (F4 TCNQ)) is up to 5 orders of magnitude larger than the mobility calculated on the basis of the first order processes (blue (TCNQ), cyan (F4 TCNQ)) for both guest molecules. In order to compare mobilities of both guest molecules, the mobility of F4 TCNQ is shifted by 0.6 eV along the *x* axis, as the LUMO level of F4 TCNQ is estimated to differ by at least 0.6 eV from the LUMO level of TCNQ. (d) Hole hopping transport in HKUST 1 loaded with TCNQ and F4 TCNQ. First order MOF−guest−MOF hopping rates for both TCNQ (green) and F4 TCNQ (black) exceed the direct MOF−MOF rate (blue) for energy differences of $\Delta E < 0.25$ eV by less than 2 orders of magnitude. Second order (superexchange) rates (red, TCNQ; orange, F4 TCNQ) are orders of magnitude below the first order MOF−MOF rates. (e) Hole mobility extracted from KMC simulations show that for $\Delta E > 0.5$ eV the mobility of the guest−host systems is the same as the mobility in the pristine HKUST 1 (blue). For $\Delta E < 0.5$ eV, the guest molecules induce a maximal increase of 1 order of magnitude for both TCNQ (solid green, no superexchange; dashed red, including superexchange) and F4 TCNQ (solid black, no superexchange; dashed yellow, including superexchange).

exchange, hopping is dominant for F4 TCNQ as well as for TCNQ. In order to compare the results for TCNQ and F4 TCNQ, we accounted for the fact that E_{gh} of F4 TCNQ is approximately 0.6 eV larger than the ΔE_{gh} of TCNQ; that is, we shifted the F4 TCNQ data to the effective energy difference in the figure. It is a natural consequence of the superexchange mechanism that the mobility for equal loading of the two guest molecules should be similar. Only in a guest−host hopping scenario, one would expect a strong difference between TCNQ and F4 TCNQ loading, as the LUMO energies of these molecules differ by 0.6 eV. As the coupling matrix elements and the reorganization energies for TCNQ and F4 TCNQ differ by less than a factor two, the conductivity of HKUST 1 loaded with either guest molecule should be comparable, which is not in agreement with prior experimental data.[16]

Because we have shown that a superexchange electron hopping mechanism can, in principle, explain the experimental data, we now investigate a hole transport mechanism analogously. Marcus hopping rates for both TCNQ and F4 TCNQ in HKUST 1 that depend on the guest−host energy difference ΔE_{gh} are displayed in Figure 3e. As the HOMO of HKUST 1 is located well above the HOMO of the guest molecules, charge transfer between MOF states dominates transport in all cases. The direct MOF−MOF rate is much larger than the rates of first order MOF−guest−MOF transfer for both systems for $\Delta E_{gh} > 0.25$ eV. For $\Delta E_{gh} < 0.25$ eV, the direct MOF−guest−MOF rates are larger than the direct MOF−MOF rates but only by up to 2 orders of magnitude. We find that superexchange hole transport does not improve the mobility across the full ΔE_{gh} range. As a result, only for ΔE_{gh} close to zero, an increase in the mobility of up to 1 order of magnitude can be expected upon loading. We, therefore, conclude that the proposed superexchange mechanism can explain the large increase of the conductivity only in the context of electron, not hole, transport.

In order to resolve the remaining inconsistency between the predicted similarity of conductivity when loading with TCNQ or with F4 TCNQ, we performed measurements of the electric conductivity of pristine and loaded high quality HKUST 1 samples using the most reliable method for the determination of conductivities of thin films, the Hg drop method.[31−34] Surface anchored MOFs (SURMOFs) were grown on a conductive substrate functionalized with a self assembled monolayer (SAM) of 9 carboxy 10 (mercaptomethyl) triptycene thiol (CMMT). These samples were prepared by liquid phase epitaxy[35,36] using the spray method[37] and

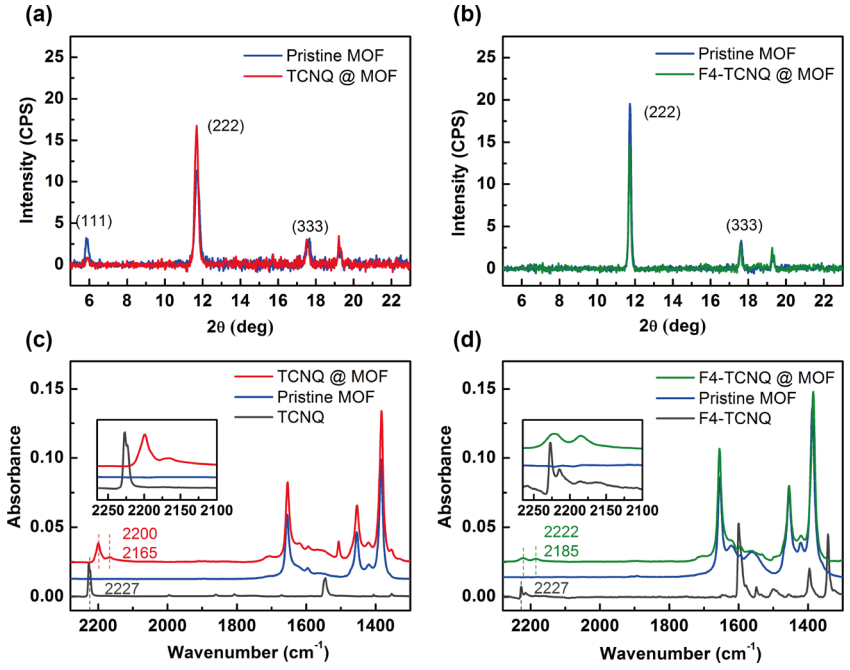

Figure 4. XRD and IRRAS data for pristine and loaded HKUST 1 SURMOFs. (a) Out of plane XRD of representative pristine (blue) and TCNQ loaded (red) SURMOF samples (5 spraying cycles). (b) Out of plane XRD of the pristine (blue curve) and F4 TCNQ loaded (green curve) SURMOFs (5 spraying cycles). (c) IRRA spectra of representative pristine (blue curve) and TCNQ loaded (red curve) HKUST 1 SURMOF samples (10 spraying cycles). A spectrum of F4 TCNQ drop casted on a Au surface is shown for comparison (black curve). Inset: Selected range of the spectra (2275 and 2100 cm^{-1}) containing the C≡N band. (d) IRRA spectra of the pristine (blue curve) and F4 TCNQ loaded (green curve) SURMOFs (5 spraying cycles). A spectrum of TCNQ drop casted on a Au surface is shown for comparison (black curve). Inset: Selected range of the spectra (2275 and 2100 cm^{-1}) containing the C≡N band.

extensively characterized by X ray diffraction (XRD), infrared and Raman spectroscopy, secondary ion mass spectroscopy, and atomic force microscopy height profiling. The SURMOF samples exhibited high quality as well as low defect densities. In addition, the crystallographic orientation along the direction perpendicular to the substrate was well defined. Thus, uncertainties and experimental artifacts, such as defects at MOF−electrode interfaces or different MOF orientations between the electrode and substrate areas expected when using bottom electrodes prefabricated by metal evaporation,[16] could be avoided. The loading of the SURMOFs by TCNQ and F4 TCNQ was performed at room temperature by their immersion in the ethanolic solutions of the guest molecules.

X ray diffraction (XRD) and infrared reflection absorption (IRRA) data for pristine and loaded SURMOFs are presented in Figure 4 for both TCNQ and F4 TCNQ. Figure 4a,b shows the out of plane XRD pattern of HKUST 1 SURMOFs prepared on the CMMT SAM modified Au substrates. The SURMOF film has the expected crystalline [111] orientation perpendicular to the substrate, as evidenced by the presence of the characteristic (111), (222), and (333) Bragg peaks with 2θ values of 5.83, 11.68, 17.58, and 23.56°, respectively. The loading with TCNQ (Figure 4a) caused no change in the SURMOF orientation or crystallinity, as evidenced by the similarity of the respective diffraction patterns (Figure 4a). The observed change in the relative intensities of the diffraction peaks can be tentatively attributed to the change of the form factor, as can be expected for homogeneous loading of the SURMOF framework with the guest molecules. The same holds true for the loading with F4 TCNQ, as depicted in Figure 4b.

Figure 4c shows the IRRA spectra of the HKUST 1 SURMOFs before and after the loading with TCNQ, along with the spectrum of TCNQ drop casted on a Au surface given for comparison. It can be seen that the characteristic absorption bands of HKUST 1, viz. COO_{asym} (1656 cm^{-1}), COO_{sym} (1455 and 1386 cm^{-1}), and signals from the benzene ring of the linker molecule (1619, 1595, and 1564 cm^{-1}) are not affected by the TCNQ loading, which suggests, in agreement with the XRD data, that the HKUST 1 framework remains intact. At the same time, upon TCNQ loading, a band around 2200 cm^{-1} appears, corresponding to the C≡N stretching mode of TCNQ and manifesting the efficiency of the loading procedure. This band, positioned at 2227 cm^{-1} for drop casted TCNQ, shifts and splits into two bands, at 2200 and 2165 cm^{-1}. These bands correspond presumably to the nonequivalent C≡N bonds involved in the bridging of the Cu^{2+} ions. Additionally, after the TCNQ loading, a new absorption band at 1354 cm^{-1} is observed, originating presumably from the C═C ring stretch of TCNQ (1353 cm^{-1}), while the C═C ring stretch of TCNQ at 1545 cm^{-1} is shifted to 1506 cm^{-1}.[38,39]

In a similar fashion, Figure 4d shows the IRRA spectra of the pristine and F4 TCNQ loaded HKUST 1 SURMOFs as well as a reference spectrum of F4 TCNQ drop casted on a Au surface. For the case of F4 TCNQ loading, we find that the intensities and positions of the characteristic absorption bands of HKUST 1 are not affected by the loading. Again, efficient loading is, however, evidenced by the appearance of the characteristic modes of F4 TCNQ in the spectra: the C≡N stretch of F4 TCNQ at 2227 cm^{-1} becomes split into two bands at 2222 and 2185 cm^{-1}, corresponding to the nonequivalent C≡N bonds that are involved in bridging the Cu^{2+} ions, as already observed for the TCNQ loading. All of these findings are supported by

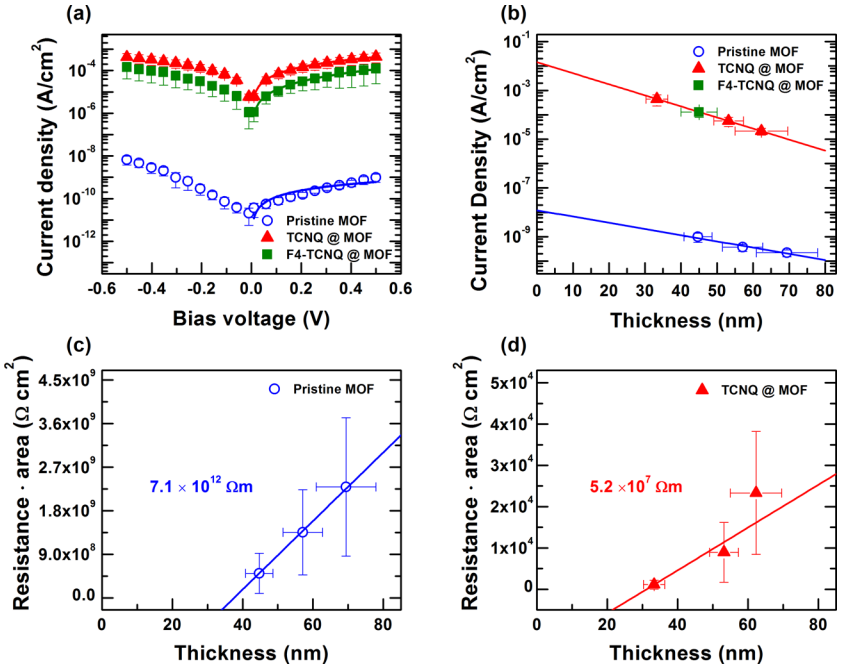

Figure 5. Experimental electric transport data for pristine and loaded HKUST 1 SURMOFs grown on the CMMT SAM. (a) Log *J vs V* plots for the pristine SURMOFs (blue open circles) as well as SURMOFs after loading with TCNQ (red solid triangles) and F4 TCNQ (green solid squares). A model for injection current was fitted to the experimental data (color coded lines). (b) Logarithm of current density at 0.5 V *vs* thickness for the pristine (blue open circles), TCNQ loaded (red solid triangles), and F4 TCNQ loaded (green solid square) SURMOFs; straight lines show linear fits. (c,d) Plot of resistance times area ($R{\cdot}A$) *vs* thickness (L) of pristine (c) and TCNQ loaded (d) SURMOFs at V = 0.5 V. Straight lines show linear fits according to $R{\cdot}A = R_c{\cdot}A + \rho{\cdot}L$, from which the resistivity ρ can be extracted.

additional Raman characterization presented in Figures S4 and S8 in the Supporting Information.

The electric conductivity of the pristine and loaded SURMOFs was measured by the Hg drop method,[31−34] where the SURMOFs were integrated into the respective junction,[15,40] with the current flowing along the direction normal to the substrate (in this direction, the SURMOFs exhibit a well defined crystallographic orientation). A detailed description of the experimental procedures as well as the results of the basic characterization and additional electric conductivity data is provided in the Supporting Information.

The major results of the electric conductivity experiments are compiled in Figure 5. In panel a, we display a semilog plot of the current density *versus* voltage for a pristine (empty) HKUST 1 prepared by five spraying cycles. AFM results for SURMOFs with different thickness are shown in the Supporting Information (Figure S3). Whereas the currents are very low for the pristine HKUST 1, as expected from the large HOMO−LUMO gap and consistent with the previous measurements,[15] upon loading with TCNQ and F4 TCNQ, the current density increases by 4−5 orders of magnitude for the both guest molecules. For TCNQ, earlier findings by Allendorf and co workers[16] are reproduced. In contrast, for F4 TCNQ, the result is distinctly different from these findings:[16] the current density is found to increase strongly and comparably to the TCNQ case upon loading, in agreement with the superexchange model.[16]

A semilog plot of the current density J at a bias voltage V = 0.5 V as a function of SURMOF thickness is presented in Figure 5b. As described in earlier work, for the pristine HKUST 1 SURMOFs, the decrease of current with thickness (or the increase of resistivity) is consistent with quasi ohmic behavior typical of metallo organic systems.[15,41,42] The obtained resistivity for the pristine HKUST 1 is about 7.1 × 10^{12} Ωm (Figure 5c), while the resistivity of the TCNQ loaded one is 5.2 × 10^7 Ωm (Figure 5d). Thus, the resistivity of HKUST 1 loaded with TCNQ is at least 5 orders lower than that for the pristine MOF. The same result was observed for F4 TCNQ, with the data point fitting almost exactly to those for the TCNQ loading. As mentioned above, this result agrees with the superexchange model but is in dissonance with the earlier findings by Allendorf and co workers.[16] The reasons for this discrepancy are presently unknown and probably related to specific parameters of both experiments. Note, however, that we have carefully excluded any possible artifacts in our work by a thorough characterization of the empty and loaded films and by the selection of a specific experimental setup for the electrical transport measurements (see above).

The reason for the poor conductivity of the pristine SURMOF is the energy of the SURMOF LUMO, which exceeds considerably the corresponding work functions of commonly used electrodes, such as Pt or Al, which are all well over 4.0 eV.[16,43] The SURMOF LUMO is mainly localized on the copper atoms of the paddle wheel unit (as shown in Figure S10 and Figure S6 of ref 16). The LUMO levels of TCNQ and F4 TCNQ are substantially closer to the Fermi energy of the electrode, thereby diminishing the injection barrier, which leads to increased conductivity upon loading.

In order to compare experimental and simulated results, we used an injection model.[44] The resulting theoretical curves (solid lines in Figure 5a) are in good agreement between the injection model and the experimental data. In order to estimate the differences between the transport level and the Fermi energy, which cannot be obtained from calculations as discussed below, we have plotted in Figure 6 the mobility resulting from this model (see the Supporting Information for

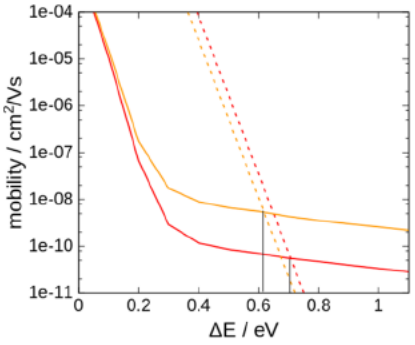

Figure 6. Mobility derived from the experimental data using an injection model (dashed lines) and KMC calculations (solid lines) as a function of the energy difference between the LUMO of the pristine *vs* the loaded SURMOF. The mobility curves intersect at approximately 0.62 and 0.71 eV for F4 TCNQ (yellow) and TCNQ (red), respectively.

details) as a function of the injection barrier differences between pristine and loaded MOF along with the mobility derived from KMC simulations. Using the intersection of theoretical and model data, we infer the injection barrier/LUMO difference between loaded and pristine MOF. The data show clearly that the observed mobility is commensurate with a difference in the LUMO level of the pristine and loaded MOF of around ~0.6 eV, which qualitatively agrees with DFT calculations. This analysis results in a difference in injection barriers between the F4 TCNQ loaded and the TCNQ loaded MOF of roughly 0.1 eV, which disagrees with the relative order of the LUMOs of these molecules in DFT calculations.

CONCLUSIONS

In summary, we have developed models for the electron and hole hopping transport through loaded MOFs and SURMOFs. For electron transport, our theoretical results yield an increase of 5 orders of magnitude in conductivity upon loading *via* the superexchange mechanism. No such effect is predicted for hole transport. The superexchange mechanism, where carriers hop from guest to guest mediated by virtual occupancy of a host site, predicts a thermally activated transport mechanism with activation energies commensurate with experimental data. The energy difference between the initial and the final state in superexchange processes is much smaller than the energy difference between the guest and the host energy levels, which results in a much larger hopping rate than for the direct hopping processes and a much weaker dependence of the conductivity on temperature. This model has important implications for the choice of suitable guest molecules to increase the conductivity of MOFs: it is a direct consequence of the superexchange model that the guest−host energy difference enters the rate only in the prefactor and not in the exponent. In the context of hopping models, it is therefore important to optimize the coupling matrix element of the guest molecule to the MOF and not the alignment of the guest and the MOF energy levels. As the coupling matrix elements of the F4 TCNQ/TCNQ to HKUST 1 are similar, the superexchange model predicts similar conductivities. To test this hypothesis, we have grown SURMOF thin films using the LPE method, yielding high quality, oriented layers with low defect density. We have performed careful experiments using the Hg drop method to demonstrate that HKUST 1 loaded with TCNQ/F4 TCNQ has orders of magnitude higher mobility than the pristine MOF, in agreement with the predictions of the superexchange scenario. We note that the kinetic MC calculations here have assumed perfectly loaded MOFs, as the experimental data suggest an efficient and homogeneous loading, but the exact loading density of the guest molecules is presently not known. Future work should therefore address the impact of the loading more precisely. From the theoretical viewpoint, a qualitative difference between the two guest molecules can be expected only when the loading approaches the percolation threshold (~35% of the sites). Further work is required to determine the sign of the Seebeck coefficient in the hopping transport model. Presently, there is no experimental or theoretical data available to quantify the difference between the Fermi and the transport energy[20] in the context of a disordered model. While to our knowledge only hopping models can rationalize the observed temperature dependence of the conductivity, it is also possible that the transport mechanism in loaded MOFs may be explained by a hybrid mechanism.

METHODS

In the Marcus theory of charge transfer, the rate for one hopping event between two sites a and b along a path is given by

$$\Gamma_{a,b} = \frac{2\pi}{\hbar}\left|J_{a,b}\right|^2 (4\pi\lambda k_B T)^{-1/2} \exp\left(-\frac{(\Delta E_{a,b} + \lambda)^2}{4\lambda k_B T}\right) \quad (1)$$

In eq 1 $J_{a,b}$ is the electronic coupling matrix element between the initial and the final states; $\Delta E_{a,b}$ is the difference between the energy levels of the molecular orbitals, and λ is the reorganization energy; k_B is the Boltzmann constant, T the temperature, and $\hbar$ the reduced Planck constant.

The total coupling matrix element describing second order superexchange charge transfer between two guest molecules g and g′ (see Figure 1b) is determined by the coupling between the initial and the intermediate host states J_{gh}^{dir} and between the intermediate and the final guest state $J_{hg'}^{dir}$ as

$$J_{gg'}^{tot} = J_{gg'}^{dir} + J_{gg'}^{sx} = J_{gg'}^{dir} + \sum_h \frac{J_{gh}^{dir} \times J_{hg'}^{dir}}{\Delta E_{sx} + \frac{1}{2}\lambda_h} \quad (2)$$

where $J_{gg'}^{dir}$ is the direct electronic coupling matrix element. $J_{gg'}^{sx}$ denotes the coupling matrix element of superexchange processes, and h denotes the virtually occupied intermediate host states. The denominator with $\Delta E_{sx} = E_h - 1/2(E_g + E_{g'})$ takes into account the fact that occupation of the virtual states is too short to allow for ionic relaxation (see the Supporting Information for details). We calculated the occupied and unoccupied orbitals of a representative fragment of the MOF/TCNQ and MOF/F4 TCNQ system using the BH LYP functional[45] and the def2 SV(P)[46] basis set as implemented in TURBOMOLE.[47] The hopping matrix elements J were calculated using the Löwdin orthogonalization[28,48] (see the Supporting Information).

For comparison of experimental and simulated data, we used an injection model where the current density depends on charge carrier concentration, mobility, and injection barrier, as

$$J(V) \sim n\mu e^{-\beta\varphi} F(V) \quad (3)$$

Here, n and μ are density of injection sites and mobility, respectively; β is the inverse product of temperature and Boltzmann constant, and φ is the height of the injection barrier. Experimental methods are presented in detail in the Supporting Information.

ASSOCIATED CONTENT

Supporting Information

The Supporting Information is available free of charge on the ACS Publications website at DOI: 10.1021/acsnano.6b03226.

Materials and methods, experimental and theoretical results (PDF)

AUTHOR INFORMATION

Corresponding Author

*E mail: wolfgang.wenzel@kit.edu.

Present Addresses

[‖]Department of Chemistry, Northwestern University, Evanston, Illinois 60208, United States.

[¶] International Iberian Nanotechnology Laboratory, Av. Mestre José Veiga, 4715 330, Braga, Portugal.

Author Contributions

[⊥]T.N., J.L., and T.W. contributed equally to this work.

Notes

The authors declare no competing financial interest.

ACKNOWLEDGMENTS

We are very grateful for discussions with P. Bobbert and A. Masse on the superexchange mechanisms. T.N. thanks the State of Baden Wuerttemberg for funding *via* Landesgraduier tenfoerderung. J.L. acknowledges the China Scholarship Council (CSC) for financial aid. V.M. thanks the European Union for funding (FP7 PEOPLE 2011 IEF; Project MOL SURMOF; No. 301110). M.Z. and T.W. thank the Deutsche Forschungsgemeinschaft for funding (Project ZH 63/14 2), W.W. acknowledges funding by the joint STW DFG project MODEOLED (WE1863/22 1) and the SFB 1176 "Struktur ierung weicher Materie" (project Q3). SIMS experiments were provided by the Karlsruhe Nano Micro Facility.

REFERENCES

(1) Zhu, Q. L.; Xu, Q. Metal Organic Framework Composites. *Chem. Soc. Rev.* **2014**, *43*, 5468−5512.

(2) Furukawa, H.; Cordova, K. E.; O'Keeffe, M.; Yaghi, O. M. The Chemistry and Applications of Metal Organic Frameworks. *Science* **2013**, *341*, 1230444.

(3) Ferey, G. Hybrid Porous Solids: Past, Present, Future. *Chem. Soc. Rev.* **2008**, *37*, 191−214.

(4) Sun, D. F.; Ma, S. Q.; Ke, Y. X.; Collins, D. J.; Zhou, H. C. An Interweaving Mof with High Hydrogen Uptake. *J. Am. Chem. Soc.* **2006**, *128*, 3896−3897.

(5) Rosi, N. L.; Eckert, J.; Eddaoudi, M.; Vodak, D. T.; Kim, J.; O'Keeffe, M.; Yaghi, O. M. Hydrogen Storage in Microporous Metal Organic Frameworks. *Science* **2003**, *300*, 1127−1129.

(6) An, J.; Rosi, N. L. Tuning Mof Co2 Adsorption Properties *Via* Cation Exchange. *J. Am. Chem. Soc.* **2010**, *132*, 5578−5579.

(7) Liu, J.; Thallapally, P. K.; McGrail, B. P.; Brown, D. R.; Liu, J. Progress in Adsorption Based Co 2 Capture by Metal−Organic Frameworks. *Chem. Soc. Rev.* **2012**, *41*, 2308−2322.

(8) Farha, O. K.; Shultz, A. M.; Sarjeant, A. A.; Nguyen, S. T.; Hupp, J. T. Active Site Accessible, Porphyrinic Metal Organic Framework Materials. *J. Am. Chem. Soc.* **2011**, *133*, 5652−5655.

(9) Shultz, A. M.; Farha, O. K.; Hupp, J. T.; Nguyen, S. T. A Catalytically Active, Permanently Microporous Mof with Metal loporphyrin Struts. *J. Am. Chem. Soc.* **2009**, *131*, 4204−4205.

(10) Kreno, L. E.; Leong, K.; Farha, O. K.; Allendorf, M.; Van Duyne, R. P.; Hupp, J. T. Metal Organic Framework Materials as Chemical Sensors. *Chem. Rev.* **2012**, *112*, 1105−1125.

(11) Lee, D. Y.; Shinde, D. V.; Yoon, S. J.; Cho, K. N.; Lee, W.; Shrestha, N. K.; Han, S. H. Cu Based Metal Organic Frameworks for Photovoltaic Application. *J. Phys. Chem. C* **2014**, *118*, 16328−16334.

(12) Kuppler, R. J.; Timmons, D. J.; Fang, Q. R.; Li, J. R.; Makal, T. A.; Young, M. D.; Yuan, D. Q.; Zhao, D.; Zhuang, W. J.; Zhou, H. C. Potential Applications of Metal Organic Frameworks. *Coord. Chem. Rev.* **2009**, *253*, 3042−3066.

(13) Stock, N.; Biswas, S. Synthesis of Metal Organic Frameworks (Mofs): Routes to Various Mof Topologies, Morphologies, and Composites. *Chem. Rev.* **2012**, *112*, 933−969.

(14) Sun, L.; Campbell, M. G.; Dincă, M. Electrically Conductive Porous Metal Organic Frameworks. *Angew. Chem., Int. Ed.* **2016**, *55*, 3566−3579.

(15) Liu, J.; Wachter, T.; Irmler, A.; Weidler, P. G.; Gliemann, H.; Pauly, F.; Mugnaini, V.; Zharnikov, M.; Woll, C. Electric Transport Properties of Surface Anchored Metal Organic Frameworks and the Effect of Ferrocene Loading. *ACS Appl. Mater. Interfaces* **2015**, *7*, 9824−30.

(16) Talin, A. A.; Centrone, A.; Ford, A. C.; Foster, M. E.; Stavila, V.; Haney, P.; Kinney, R. A.; Szalai, V.; El Gabaly, F.; Yoon, H. P.; Leonard, F.; Allendorf, M. D. Tunable Electrical Conductivity in Metal Organic Framework Thin Film Devices. *Science* **2014**, *343*, 66−69.

(17) Bässler, H. Charge Transport in Disordered Organic Photo conductors a Monte Carlo Simulation Study. *Phys. Status Solidi B* **1993**, *175*, 15−56.

(18) Ahrenholtz, S. R.; Epley, C. C.; Morris, A. J. Solvothermal Preparation of an Electrocatalytic Metalloporphyrin Mof Thin Film and Its Redox Hopping Charge Transfer Mechanism. *J. Am. Chem. Soc.* **2014**, *136*, 2464−2472.

(19) Erickson, K. J.; Léonard, F.; Stavila, V.; Foster, M. E.; Spataru, C. D.; Jones, R. E.; Foley, B. M.; Hopkins, P. E.; Allendorf, M. D.; Talin, A. A. Thin Film Thermoelectric Metal−Organic Framework with High Seebeck Coefficient and Low Thermal Conductivity. *Adv. Mater.* **2015**, *27*, 3453−3459.

(20) Ihnatsenka, S.; Crispin, X.; Zozoulenko, I. V. Understanding Hopping Transport and Thermoelectric Properties of Conducting Polymers. *Phys. Rev. B: Condens. Matter Mater. Phys.* **2015**, *92*, 035201.

(21) Minder, N. A.; Ono, S.; Chen, Z. H.; Facchetti, A.; Morpurgo, A. F. Band Like Electron Transport in Organic Transistors and Implication of the Molecular Structure for Performance Optimization. *Adv. Mater.* **2012**, *24*, 503.

(22) Morisaki, H.; Koretsune, T.; Hotta, C.; Takeya, J.; Kimura, T.; Wakabayashi, Y. Large Surface Relaxation in the Organic Semi conductor Tetracene. *Nat. Commun.* **2014**, *5*, 5400.

(23) Rajeswaran, M.; Blanton, T. N.; Tang, C. W.; Lenhart, W. C.; Switalski, S. C.; Giesen, D. J.; Antalek, B. J.; Pawlik, T. D.; Kondakov, D. Y.; Zumbulyadis, N.; Young, R. H. Structural, Thermal, and Spectral Characterization of the Different Crystalline Forms of Alq3, Tris(Quinolin 8 Olato)Aluminum(Iii), an Electroluminescent Material in Oled Technology. *Polyhedron* **2009**, *28*, 835−843.

(24) Marcus, R. A. Electron Transfer Reactions in Chemistry. Theory and Experiment. *Rev. Mod. Phys.* **1993**, *65*, 599−610.

(25) Jortner, J.; Bixon, M.; Voityuk, A. A.; Rösch, N. Superexchange Mediated Charge Hopping in DNA. *J. Phys. Chem. A* **2002**, *106*, 7599−7606.

(26) Allendorf, M. D.; Foster, M. E.; Léonard, F.; Stavila, V.; Feng, P. L.; Doty, F. P.; Leong, K.; Ma, E. Y.; Johnston, S. R.; Talin, A. A. Guest Induced Emergent Properties in Metal−Organic Frameworks. *J. Phys. Chem. Lett.* **2015**, *6*, 1182−1195.

(27) Rodin, V.; Symalla, F.; Meded, V.; Friederich, P.; Danilov, D.; Poschlad, A.; Nelles, G.; von Wrochem, F.; Wenzel, W. Generalized Effective Medium Model for the Carrier Mobility in Amorphous Organic Semiconductors. *Phys. Rev. B: Condens. Matter Mater. Phys.* **2015**, *91*, 155203.

(28) Stehr, V.; Pfister, J.; Fink, R.; Engels, B.; Deibel, C. First Principles Calculations of Anisotropic Charge Carrier Mobilities in Organic Semiconductor Crystals. *Phys. Rev. B: Condens. Matter Mater. Phys.* **2011**, *83*, 155208.

(29) Nelsen, S. F.; Blackstock, S. C.; Kim, Y. Estimation of Inner Shell Marcus Terms for Amino Nitrogen Compounds by Molecular Orbital Calculations. *J. Am. Chem. Soc.* **1987**, *109*, 677−682.

(30) Gu, Z. G.; Heinke, L.; Wöll, C.; Neumann, T.; Wenzel, W.; Li, Q.; Fink, K.; Gordan, O. D.; Zahn, D. R. Experimental and Theoretical Investigations of the Electronic Band Structure of Metal Organic Frameworks of Hkust 1 Type. *Appl. Phys. Lett.* **2015**, *107*, 183301.

(31) Rampi, M. A.; Schueller, O. J. A.; Whitesides, G. M. Alkanethiol Self Assembled Monolayers as the Dielectric of Capacitors with Nanoscale Thickness. *Appl. Phys. Lett.* **1998**, *72*, 1781−1783.
(32) Haag, R.; Rampi, M. A.; Holmlin, R. E.; Whitesides, G. M. Electrical Breakdown of Aliphatic and Aromatic Self Assembled Monolayers Used as Nanometer Thick Organic Dielectrics. *J. Am. Chem. Soc.* **1999**, *121*, 7895−7906.
(33) Holmlin, R. E.; Haag, R.; Chabinyc, M. L.; Ismagilov, R. F.; Cohen, A. E.; Terfort, A.; Rampi, M. A.; Whitesides, G. M. Electron Transport through Thin Organic Films in Metal Insulator Metal Junctions Based on Self Assembled Monolayers. *J. Am. Chem. Soc.* **2001**, *123*, 5075−5085.
(34) Tran, E.; Rampi, M. A.; Whitesides, G. M. Electron Transfer in a Hg Sam//Sam Hg Junction Mediated by Redox Centers. *Angew. Chem., Int. Ed.* **2004**, *43*, 3835−3839.
(35) Zacher, D.; Shekhah, O.; Wöll, C.; Fischer, R. A. Thin Films of Metal Organic Frameworks. *Chem. Soc. Rev.* **2009**, *38*, 1418−1429.
(36) Shekhah, O.; Wang, H.; Kowarik, S.; Schreiber, F.; Paulus, M.; Tolan, M.; Sternemann, C.; Evers, F.; Zacher, D.; Fischer, R. A.; Wöll, C. Step by Step Route for the Synthesis of Metal Organic Frame works. *J. Am. Chem. Soc.* **2007**, *129*, 15118−15119.
(37) Arslan, H. K.; Shekhah, O.; Wohlgemuth, J.; Franzreb, M.; Fischer, R. A.; Wöll, C. High Throughput Fabrication of Uniform and Homogenous Mof Coatings. *Adv. Funct. Mater.* **2011**, *21*, 4228−4231.
(38) Maiti, S.; Maiti, U. N.; Pal, S.; Chattopadhyay, K. K. Organic Nanowire Hierarchy over Fabric Platform for Flexible Cold Cathode. *Nanotechnology* **2013**, *24*, 465601.
(39) Takenaka, T. Infrared and Raman Spectra of Tcnq and Tcnq D4 Crystals. *Bull. Inst. Chem. Res.* **1969**, *47*, 387−400.
(40) Querebillo, C. J.; Terfort, A.; Allara, D. L.; Zharnikov, M. Static Conductance of Nitrile Substituted Oligophenylene and Oligo (Phenylene Ethynylene) Self Assembled Monolayers Studied by the Mercury Drop Method. *J. Phys. Chem. C* **2013**, *117*, 25556−25561.
(41) Tuccitto, N.; Ferri, V.; Cavazzini, M.; Quici, S.; Zhavnerko, G.; Licciardello, A.; Rampi, M. A. Highly Conductive∼ 40 Nm Long Molecular Wires Assembled by Stepwise Incorporation of Metal Centres. *Nat. Mater.* **2009**, *8*, 41−46.
(42) Musumeci, C.; Zappalà, G.; Martsinovich, N.; Orgiu, E.; Schuster, S.; Quici, S.; Zharnikov, M.; Troisi, A.; Licciardello, A.; Samorì, P. Nanoscale Electrical Investigation of Layer by Layer Grown Molecular Wires. *Adv. Mater.* **2014**, *26*, 1688−1693.
(43) Skriver, H. L.; Rosengaard, N. M. Surface Energy and Work Function of Elemental Metals. *Phys. Rev. B: Condens. Matter Mater. Phys.* **1992**, *46*, 7157−7168.
(44) Shen, Y.; Klein, M. W.; Jacobs, D. B.; Campbell Scott, J.; Malliaras, G. G. Mobility Dependent Charge Injection into an Organic Semiconductor. *Phys. Rev. Lett.* **2001**, *86*, 3867−3870.
(45) Becke, A. D. A New Mixing of Hartree−Fock and Local Density Functional Theories. *J. Chem. Phys.* **1993**, *98*, 1372−1377.
(46) Schäfer, A.; Horn, H.; Ahlrichs, R. Fully Optimized Contracted Gaussian Basis Sets for Atoms Li to Kr. *J. Chem. Phys.* **1992**, *97*, 2571−2577.
(47) Ahlrichs, R.; Bär, M.; Häser, M.; Horn, H.; Kölmel, C. Electronic Structure Calculations on Workstation Computers: The Program System Turbomole. *Chem. Phys. Lett.* **1989**, *162*, 165−169.
(48) Löwdin, P. O. On the Non Orthogonality Problem Connected with the Use of Atomic Wave Functions in the Theory of Molecules and Crystals. *J. Chem. Phys.* **1950**, *18*, 365−375.